Available online at www.sciencedirect.com
ScienceDirect
Journal of Sound and Vibration 320 (2009) 878–892
JOURNAL OF SOUND AND VIBRATION
www.elsevier.com/locate/jsvi

Multiple scattering of flexural waves from a cylindrical inclusion in a semi-infinite thin plate

Xue-Qian Fang[a,*], Xiao-Hua Wang[b]

[a]*Department of Engineering Mechanics, Shijiazhuang Railway Institute, Shijiazhuang 050043, PR China*
[b]*Computer and Information Engineering Department, Shijiazhuang Railway Institute, Shijiazhuang 050043, PR China*

Received 13 April 2008; received in revised form 30 July 2008; accepted 21 August 2008
Handling Editor: J. Lam
Available online 2 October 2008

Abstract

In this paper, image method and wave function expansion method are applied to investigate the multiple scattering of flexural waves and dynamic stress concentration from a cylindrical inclusion in a semi-infinite thin plate, and the analytical solution of this problem is obtained. The semi-infinite plate with roller-supported boundary is considered, and the image method is used to satisfy the boundary condition. The addition theorem for Bessel functions is employed to accomplish the translation of wave fields between different local coordinate systems. As an example, the numerical results of dynamic stress concentration factors around the inclusion are graphically presented and analyzed. Analysis shows that the angular distribution of the dynamic stress around the inclusion shows great difference when the distance between the inclusion and the semi-infinite edge is different. The effects of the elastic modulus, density, Poisson's ratio, and the thickness of the inclusion on the shadow side of the inclusion are greater when the distance between inclusion and the semi-infinite edge is small. In the region of lower frequency, the effects of the elastic modulus, density, Poisson's ratio, and the thickness of the inclusion on the dynamic stress are little. Comparisons with other existing models are also discussed.

1. Introduction

Plate structures are widely used in aviation, aerospace, shipping, and civil construction engineering. Inhomogeneities such as inclusions, cavities, or cracks in plates strongly affect the serving life of the structure. If the inhomogeneities are embedded in a plate, it is definitely vital to determine them and analyze their effects. The knowledge of stress concentration analysis is very important for a reliable design of the plate, so the stress concentration problems in the plate have received a considerable amount of interest over the past few decades.

It is known from the literature on wave dynamics that in a certain range of wave frequency, the dynamic stress around the inhomogeneities is much greater than the static stress. So, to increase the bearing capacity of structures and the service life of structures, the investigations on elastic waves scattering and dynamic stress concentrations in plate structures are more important.

*Corresponding author. Tel.: +86 311 87936542.
E-mail address: fangxueqian@yahoo.com.cn (X.-Q. Fang).

0022-460X/$ - see front matter © 2008 Elsevier Ltd. All rights reserved.
doi:10.1016/j.jsv.2008.08.023

Up to present time, stress concentration caused by cutouts or inclusions in an infinite plate has been an interesting research topic. First, Kirsch [1] pioneered the study of the stress concentration around a circular hole in the infinite plate under a uniform longitudinal tension. Subsequently, Ying and Truell [2] studied the scattering of sound waves by a spherical scatterer in an elastic medium. Kato [3] and White [4] considered the effect of a cylindrical obstacle on wave scattering. Afterwards, Pao and Chao [5] and Pao [6] investigated the flexural wave diffractions by a cavity in an elastic plate based on Mindlin's theory. Using a combined finite element and analytical method, Paskaramoorthy et al. studied the scattering of slow flexural waves by arbitrary-shaped cavities [7] and a finite through-crack [8] in the infinite elastic plate. The analogous problem of scattering of flexural waves by circular inclusions was solved by Vemula and Norris using the Mindlin plate theory [9] as well as the lower-order Kirchhoff plate theory [10]. Recently, Leviatan et al. [11] presented a source-model technique to investigate the scattering of time-harmonic flexural wave in a heterogeneous thin plate.

To the author's knowledge, the researches on flexural waves and dynamic stress in plates mainly focused on the models of infinite structures. However, the models of semi-infinite plates are more familiar in engineering application [12]. Due to the complexity of multiple scattering and reflection of elastic waves between the inhomogeneities and the boundary, an alternative, and possibly simpler, point of view is to ignore edge effects as a first approximation. This approach is only suitable for large plates with distant edges, and leads to much simplification. To accurately describe the dynamic stress distribution, the boundary effect of the plate should be considered. In the past, only a few papers about the dynamic stress in the semi-infinite plate are reported. The scattering of time-harmonic plane longitudinal, shear, and Rayleigh waves by a crack in two dimensions embedded in a homogeneous isotropic elastic half-space was investigated by Shah et al. [13]. In a series of detailed study, Fang and his co-workers have investigated the multiple scattering and reflection of anti-plane shear waves from cavities in the semi-infinite plate [14,15] and a semi-infinite slab [16], and the boundary effect were analyzed.

The multiple scattering and reflection of flexural waves at the boundary of plates are more complicated than those of single-mode waves such as the acoustic and shear waves due to the generation of non-geometrically induced evanescent waves and the effects of higher-order boundary conditions [17]. Therefore, very few papers have investigated this problem. Only recently, Fang and his co-workers have studied the multiple scattering of flexural waves from a cutout [18] and two cutouts [19] in the semi-infinite plate.

The main objective of this paper is to extend the work of Hu et al. [18] to the case of the multiple scattering of flexural waves from an embedded inclusion in a semi-infinite thin plate with roller-supported boundary. The image method is applied to satisfy the boundary conditions of the semi-infinite structure. Based on Mindlin's theory of transverse motion in thin plates, the wave function expansion method is employed to express the wave fields around the actual and image inclusions. The analytical solutions of the problem are obtained. As an example, the numerical results of dynamic stress concentration factor (DSCF) around the inclusion are graphically presented and discussed.

2. Governing equation of flexural waves in thin plates and its solution

Consider a semi-infinite thin plate with a cylindrical inclusion, which is perfectly bonded to the exterior region along the boundary of the inclusion, as depicted in Fig. 1. For simplicity, the properties of the inclusion are assumed to be uniform through their thickness. Let D, ρ, and h be the bending stiffness, density and thickness of the plate, and D_0, ρ_0, and h_0 those of the inclusion. The radius of the cylindrical inclusion is a. The distance between the center of the inclusion and the semi-infinite edge is d. The incidence of plane flexural waves over the surface of the semi-infinite thin plate in the x direction is considered.

For sufficiently thin plates, approximate theories are applied. These theories take into account that the plate is thin and so the dependency of displacement field on the thickness coordinate may be neglected or supposed to be polynomial. Mindlin's approximate theory for flexural waves in plates is well known, and can be found in many textbooks, for example [17,20]. The theory includes shear-deformation and rotary-inertia effects, as in the Timoshenko beam theory.

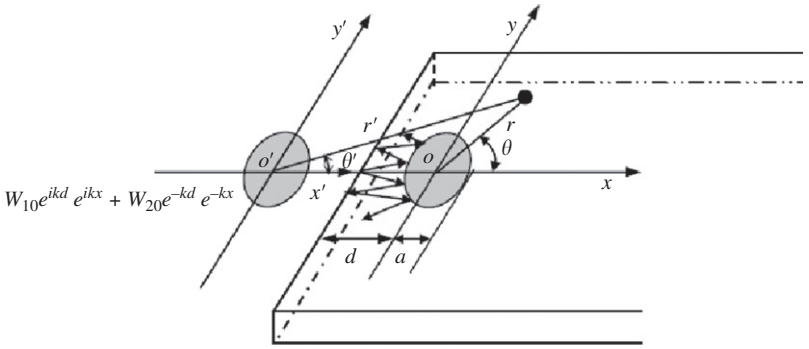

Fig. 1. Sketch of elastic waves incident upon a semi-infinite plate with a cylindrical inclusion.

Based on Mindlin's theory, the flexural wave equation in elastic thin plates may be described as [20]

$$D\nabla^2\nabla^2 w + \rho h\frac{\partial^2 w}{\partial t^2} = q, \tag{1}$$

where t is the time, q the externally applied transverse pressure, w the transverse displacement, and D the bending stiffness of the plate with

$$D = Eh^3/12(1-v^2) \tag{2}$$

in which E, v, h are the elastic modulus, Poisson's ratio, and thickness of the plate. In the case of this paper, q is defined as $q = 0$.

Steady periodic solutions of the problem are investigated. Let $w = \mathrm{Re}[W\exp(-\mathrm{i}\omega t)]$, then the displacement components determined by steady flexural waves are

$$u_x = -z\frac{\partial w}{\partial x}, \quad u_y = -z\frac{\partial w}{\partial y}, \quad u_z = w = \mathrm{Re}[W(x,y)\mathrm{e}^{-\mathrm{i}\omega t}], \tag{3}$$

where ω is the incident frequency, $\mathrm{Re}(\cdot)$ denotes the real part, and $\mathrm{i} = \sqrt{-1}$ is the imaginary unit.

According to Eqs. (1) and (3), $W(x, y)$ should satisfy the following equations:

$$\nabla^2\nabla^2 W - k^4 W = (\nabla^2 + k^2)(\nabla^2 - k^2)W = 0, \tag{4}$$

$$(\nabla^2 + k^2)W_1 = 0 \quad (\nabla^2 - k^2)W_2 = 0. \tag{5}$$

Here, k is the wavenumber of elastic waves in the plate, and $k = (\rho h\omega^2/D)^{1/4}$.

In Eq. (5), it is noted that $W_1\mathrm{e}^{-\mathrm{i}\omega t}$ denotes the propagating elastic waves in plates and $W_2\mathrm{e}^{-\mathrm{i}\omega t}$ denotes the localized evanescent wave motion. The two parts are integrated and form the motion of flexural waves and vibration modes in thin plates.

According to Eq. (4), the general solution of the scattered waves resulting from the cylindrical inclusion can be described as

$$W^s = W_1^s + W_2^s = \sum_{n=-\infty}^{\infty}[A_n^1 H_n^{(1)}(kr)\mathrm{e}^{\mathrm{i}n\theta} + A_n^2 K_n(kr)\mathrm{e}^{\mathrm{i}n\theta}], \tag{6}$$

where A_n^1 and A_n^2 are determined by satisfying the boundary conditions are the mode coefficients of scattered waves from inclusions, $H_n^{(1)}(\cdot)$ is the nth-order Hankel function of the first kind, and $K_n(\cdot)$ is the nth-order modified Bessel function of the second kind. The superscript s denotes the scattered waves. It should be noted that $H_n^{(1)}(\cdot)$ and $K_n(\cdot)$ denote the outgoing waves.

Likewise, the refracted wave field in the inclusion is a standing wave, which can be described as

$$W^r = W_1^r + W_2^r = \sum_{n=-\infty}^{\infty}[C_{n1}J_n(k_0 r)\mathrm{e}^{\mathrm{i}n\theta} + C_{n2}I_n(k_0 r)\mathrm{e}^{\mathrm{i}n\theta}], \tag{7}$$

where $k_0 = (\rho_0 h_0 \omega^2 / D_0)^{1/4}$ is the wavenumber of elastic waves in the inclusion, C_{n1} and C_{n2} determined by satisfying the boundary conditions are the mode coefficients of refracted waves from inclusions, $J_n(\cdot)$ is the nth-order Bessel function of the first kind, and $I_n(\cdot)$ is the nth-order modified Bessel function of the first kind. The superscript r denotes the refracted waves.

3. Excitation of incident waves and total wave field in the plate

Assume that a plane flexural wave propagates along the positive x direction in the semi-infinite plate. One is the propagating wave and the other is the localized vibration. According to the wave function expansion method, the incident waves may be described as

$$\begin{aligned} W_1^i &= W_{10} e^{ikd} e^{ikx} + W_{20} e^{-kd} e^{-kx} \\ &= W_{10} e^{ikd} \sum_{n=-\infty}^{\infty} i^n J_n(kr) e^{in\theta} + W_{20} e^{-kd} \sum_{n=-\infty}^{\infty} I_n(kr) e^{in\theta}, \end{aligned} \tag{8}$$

where W_{10}, W_{20} are the transverse vibration amplitudes of incident flexural waves. Note that the superscript i denotes the incident waves.

When the flexural wave propagates in the semi-infinite structure, it is scattered by the inclusion at first. Then, the outgoing scattered wave from the inclusion is reflected by the semi-infinite edge, and the reflected waves W_1^f arise. The reflected waves are scattered by the inclusion again. This complex phenomenon is shown in Fig. 1.

A semi-infinite thin plate with roller-supported boundary is considered. To satisfy the boundary conditions at the semi-infinite edge, the image method is applied. The reflected waves at the edge of the semi-infinite plate are described by the virtual image inclusion. For the image inclusion, the incident flexural waves propagate in the negative x' direction, and can be expressed as

$$\begin{aligned} W_2^i &= W_{10} e^{ikd} e^{-ikx'} + W_{20} e^{-kd} e^{kx'} \\ &= W_{10} e^{ikd} \sum_{n=-\infty}^{\infty} i^{-n} J_n(kr') e^{in\theta'} + W_{20} e^{-kd} \sum_{n=-\infty}^{\infty} (-1)^n I_n(kr') e^{in\theta'}. \end{aligned} \tag{9}$$

When the exciting source is enough far from the inclusions, one may consider $W_{20} = 0$, and then the incident waves for the actual and image inclusions are described as

$$W_1^i = W_{10} e^{ikd} e^{ikx} = W_{10} e^{ikd} \sum_{n=-\infty}^{\infty} i^n J_n(kr) e^{in\theta}, \tag{10}$$

$$W_2^i = W_{10} e^{ikd} e^{-ikx'} = W_{10} e^{ikd} \sum_{n=-\infty}^{\infty} i^{-n} J_n(kr') e^{in\theta'}. \tag{11}$$

Considering the multiple scattering between the actual and image inclusions, the scattered fields of flexural waves produced by the actual inclusion in the localized coordinate system (r, θ) are described as

$$W_1^s = \sum_{n=-\infty}^{\infty} \bar{A}_{n1} H_n^{(1)}(kr) e^{in\theta} + \sum_{n=-\infty}^{\infty} \bar{A}_{n2} K_n(kr) e^{in\theta}, \tag{12}$$

where $\bar{A}_{nj} = \sum_{l=1}^{\infty} A_{nj}^l$ for $j = 1, 2$ are the total scattering coefficients of the actual inclusion, and the superscript s denotes the scattered waves. Note that l denotes the lth mode coefficients of scattered waves.

Similarly, the scattered waves produced by the image inclusion in the localized coordinate system (r', θ'), are described as

$$W_2^s = \sum_{n=-\infty}^{\infty} \bar{B}_{n1} H_n^{(1)}(kr') e^{in\theta'} + \sum_{n=-\infty}^{\infty} \bar{B}_{n2} K_n(kr') e^{in\theta'}, \tag{13}$$

where $\bar{B}_{n1}, \bar{B}_{n2}$ are the total mode coefficients of scattered waves of the image inclusion. They are determined by satisfying the boundary conditions of the inclusions. In fact, they are also related to the boundary conditions of the edge of plates.

From Eqs. (10) and (11), the total incident wave W_t^i, the original incident wave plus its image as the reflected wave from the roller-supported edge, can be written as

$$W_t^i = W_{10}\mathrm{e}^{\mathrm{i}kd}(\mathrm{e}^{\mathrm{i}kx} + \mathrm{e}^{-\mathrm{i}kx'}) = W_{10}\mathrm{e}^{\mathrm{i}kd}\left[\sum_{n=-\infty}^{\infty}(\mathrm{i}^n + \mathrm{e}^{-2\mathrm{i}kd}\mathrm{i}^{-n})J_n(kr)\mathrm{e}^{\mathrm{i}n\theta}\right]. \tag{14}$$

Then, the total field of elastic waves in the semi-infinite plate should be produced by the superposition of the incident field, the scattered fields and the reflected fields at the edge of the plate, i.e.,

$$W = W_1^i + W_1^s + W_1^f = W_1^i + W_1^s + W_2^s. \tag{15}$$

Now, for the straight roller-supported edge, the boundary conditions at the edge are considered:

$$\frac{\partial W^{(t)}}{\partial x} = \frac{\partial^3 W^{(t)}}{\partial x^3} = 0 \quad \text{at } x = -b. \tag{16}$$

From Eq. (14), it is clear that the total incident wave has satisfied these conditions.

Applying the boundary conditions (16) to Eq. (15), and from the fact that $r = r'$, $\theta' = \pi - \theta$ on the plane boundary of the semi-infinite structure, and the identity $H_n^{(1)}\mathrm{e}^{\mathrm{i}n\pi} = H_{-n}^{(1)}$, the following relations between the total mode coefficients of scattered waves are obtained:

$$\bar{B}_{n1} = \bar{A}_{-n1}, \quad \bar{B}_{n2} = (-1)^{-n}\bar{A}_{-n2}. \tag{17}$$

From Eq. (17), the relations between the total scattering coefficients of the image inclusion and those of the actual inclusion are obtained.

Then, by using the following translational addition theorems of Bessel functions [21]

$$H_n^{(1)}(kr')\mathrm{e}^{\mathrm{i}n\theta'} = \sum_{m=-\infty}^{\infty}(-1)^{m-n}H_{m-n}^{(1)}(2kd)J_m(kr)\mathrm{e}^{\mathrm{i}m\theta}, \tag{18}$$

$$K_n(kr')\mathrm{e}^{\mathrm{i}n\theta'} = \sum_{m=-\infty}^{\infty}(-1)^{m}K_{m-n}(2kd)I_m(kr)\mathrm{e}^{\mathrm{i}m\theta}, \tag{19}$$

the scattered fields W_2^s of the image inclusion can be represented in the local coordinate systems (r, θ).

After some manipulations, the total scattered field W^s around the actual inclusion is expressed as

$$\begin{aligned} W^s = &\sum_{n=-\infty}^{\infty}\bar{A}_{n1}H_n^{(1)}(kr)\mathrm{e}^{\mathrm{i}n\theta} + \sum_{n=-\infty}^{\infty}\sum_{m=-\infty}^{\infty}\bar{A}_{m1}\hbar_{mn}J_n(kr)\mathrm{e}^{\mathrm{i}n\theta} \\ &+ \sum_{n=-\infty}^{\infty}\bar{A}_{n2}K_n(kr)\mathrm{e}^{\mathrm{i}n\theta} + \sum_{n=-\infty}^{\infty}\sum_{m=-\infty}^{\infty}\bar{A}_{m2}\kappa_{mn}I_n(kr)\mathrm{e}^{\mathrm{i}n\theta}, \end{aligned} \tag{20}$$

where

$$\hbar_{mn} = (-1)^{n+m}H_{n+m}^{(1)}(2kd) \quad \text{and} \quad k_{mn} = (-1)^{n+m}K_{n+m}^{(1)}(2kd).$$

4. Boundary conditions around the inclusion in the plate

There are four continuous conditions around the inclusion. It is required that W^t, $\partial W^t/\partial r$, M_{rr} and V_r are continuous across the boundary of the inclusion. The expressions of M_{rr} and V_r are given by

$$M_{rr} = -D\left[\frac{\partial^2 W^t}{\partial r^2} + v\left(\frac{1}{r}\frac{\partial W^t}{\partial r} + \frac{1}{r^2}\frac{\partial^2 W^t}{\partial \theta^2}\right)\right], \tag{21}$$

$$V_r = Q_r + \frac{1}{r}\frac{\partial M_{r\theta}}{\partial \theta} = -D\frac{\partial}{\partial r}(\nabla^2 W^t) - D(1-v)\frac{1}{r^2}\frac{\partial}{\partial \theta}\left(\frac{\partial^2 W^t}{\partial r \partial \theta} - \frac{1}{r}\frac{\partial W^t}{\partial \theta}\right), \tag{22}$$

where M_{rr} and V_r are the bending moment and the equivalent shear force around the inclusions, respectively.

5. Solution of scattering mode coefficients of elastic waves

By substituting the expressions of wave fields into the boundary conditions of the actual inclusion, four equations determining the mode coefficients are obtained. Multiplying by $e^{-is\theta}$ and integrating from 0 to 2π on both sides of the equations, one can obtain a set of system of linear equations for the unknown mode coefficients $\{\bar{A}_{n1}, \bar{A}_{n2}, C_{n1}, C_{n2}\}$,

$$\begin{aligned}&\bar{A}_{n1}H_n^{(1)}(ka) + J_n(ka)\sum_{m=-\infty}^{\infty}\hbar_{mn}\bar{A}_{m1} + K_n(ka)\bar{A}_{n2} + I_n(ka)\sum_{m=-\infty}^{\infty}\kappa_{mn}\bar{A}_{m2}\\ &- J_n(k_0a)C_{n1} - I_n(k_0a)C_{n2} = -W_{10}e^{ikd}(i^n + e^{-2ikd}i^{-n})J_n(ka),\end{aligned} \tag{23}$$

$$\begin{aligned}&\bar{A}_{n1}\hbar_H^1 + \hbar_J^1\sum_{m=-\infty}^{\infty}\hbar_{mn}\bar{A}_{m1} + \hbar_K^1\bar{A}_{n2} + \hbar_I^1\sum_{m=-\infty}^{\infty}\kappa_{mn}\bar{A}_{m2}\\ &- \hbar_J^2 C_{n1} - \hbar_I^2 C_{n2} = -W_{10}e^{ikd}(i^n + e^{-2ikd}i^{-n})\hbar_J^1,\end{aligned} \tag{24}$$

$$\begin{aligned}&\Re_H^1\bar{A}_{n1} + \Re_J^1\sum_{m=-\infty}^{\infty}\hbar_{mn}\bar{A}_{m1} + \Re_K^1\bar{A}_{n2} + \Re_I^1\sum_{m=-\infty}^{\infty}\kappa_{mn}\bar{A}_{m2} - \frac{D_0}{D}[\Re_J^2 C_{n1} + \Re_I^2 C_{n2}]\\ &= -W_{10}e^{ikd}(i^n + e^{-2ikd}i^{-n})\Re_J^1,\end{aligned} \tag{25}$$

$$\begin{aligned}&\Im_H^1\bar{A}_{n1} + \Im_J^1\sum_{m=-\infty}^{\infty}\hbar_{mn}\bar{A}_{m1} + \Im_K^1\bar{A}_{n2} + \Im_I^1\sum_{m=-\infty}^{\infty}\kappa_{mn}\bar{A}_{m2} - \frac{D_0}{D}[\Im_J^2 C_{n1} + \Im_I^2 C_{n2}]\\ &= -W_{10}e^{ikd}(i^n + e^{-2ikd}i^{-n})\Im_J^1.\end{aligned} \tag{26}$$

Here, the following notations are used:

$$\hbar_X^1 = [nX_n(ka) \mp kaX_{n+1}(ka)], \tag{27}$$

$$\hbar_X^2 = [nX_n(k_0a) \mp k_0aX_{n+1}(k_0a)], \tag{28}$$

$$\Re_X^1 = [n^2(1-v) \mp (ka)^2]X_n(ka) - (1-v)kaX_n'(ka), \tag{29}$$

$$\Re_X^2 = [n^2(1-v_0) \mp (k_0a)^2]X_n(k_0a) - (1-v_0)k_0aX_n'(k_0a), \tag{30}$$

$$\Im_X^1 = n^2(1-v)X_n(ka) - [n^2ka(1-v) \mp (ka)^3]X_n'(ka), \tag{31}$$

$$\Im_X^2 = n^2(1-v_0)X_n(k_0a) - [n^2k_0a(1-v_0) \mp (k_0a)^3]X_n'(k_0a), \tag{32}$$

where the upper and lower signs refer to $X = H^{(1)}$, J and $X = K$, I, respectively.

After arrangement, Eqs. (23)–(26) can be simplified as

$$\mathbf{EA} = \mathbf{f}, \tag{33}$$

where $\mathbf{E}$ is the coefficient matrix of $(8n+4)\times(8n+4)$, $\mathbf{f}$ the vector of $(8n+4)$ ranks, and $\mathbf{A}$ the mode coefficients.

According to the definition of DSCF, the dynamical bending moment concentration factor is the ratio of amplitude hoop bending moment around the inclusion and the maximum bending moment in the incident direction of elastic waves [22]. Thus, the expression of the DSCF around the cylindrical inclusion

described as

$$\mathrm{DSCF} = M^*_{\theta\theta} = M_{\theta\theta}/M_0 = -\frac{1}{W_{10}k^2}[\nabla^2 W - (1-v)\partial^2 W/\partial r^2], \tag{34}$$

where M_0 is the maximum amplitude of bending moment of incident waves and $M_0 = Dk^2 W_{10}$.

Then, the DSCF around the inclusions a and b are, respectively, written as

$$\mathrm{DSCF} = \frac{1}{k^2a^2}\left[e^{ikd}\sum_{n=-\infty}^{\infty}(i^n + e^{-2ikd}i^{-n})T_J e^{in\theta} + \sum_{n=-\infty}^{\infty}\bar{A}_{n1}T_H e^{in\theta} + \sum_{n=-\infty}^{\infty}\sum_{m=-\infty}^{\infty}\bar{A}_{m1}\hbar^{(1)}_{mn}T_J e^{in\theta} + \sum_{n=-\infty}^{\infty}\bar{A}_{n2}T_K e^{in\theta} + \sum_{n=-\infty}^{\infty}\sum_{m=-\infty}^{\infty}\bar{A}_{m2}\kappa^{(1)}_{mn}T_I e^{in\theta}\right]. \tag{35}$$

Here, the following notations are used:

$$T_X = (1-v)kaX'_n(ka) - [(1-v)n^2 \pm v(ka)^2]X_n(ka), \tag{36}$$

where the upper and lower signs refer to $X = H^{(1)}$, J and $X = K$, I, respectively.

6. Numerical examples and discussion

Fatigue failures often occur in the regions with high stress concentration, so an understanding of the distribution of the dynamic stress around the inclusion is quite useful in structural design. According to the expression of DSCF, the DSCFs around the cylindrical inclusion are simulated by using MATLAB.

In the following analysis, it is convenient to make the variables dimensionless. To accomplish this step, a representative length scale a, where a is the radius of inclusion, is introduced. The following dimensionless variables and quantities have been chosen for computation: the incident wavenumber is $k^* = ka = 0.01$–2.0, the distance between the center of the inclusion and the semi-infinite boundary is $d^* = d/a = 1.1$–10.0, the ratio of elastic modulus $E^* = E_0/E = 0.1$–5.0, the ratio of mass density $\rho^* = \rho_0/\rho = 0.1$–$2.0$, the ratio of thickness $h^* = h_0/h = 1.0$–2.0, $v = 0.3$, and $v_0 = 0.2$, 0.3, 0.4.

To validate the present dynamical model, Figs. 2 and 3 are given. Fig. 2 shows the angular distribution of the DSCFs around a hole in the infinite thin plate. The DSCFs obtained from Ref. [7] are represented by line

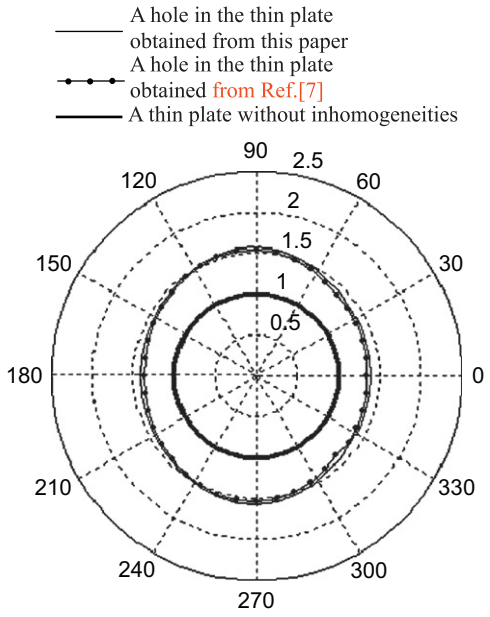

Fig. 2. Comparison of the angular distribution of dynamic stress concentration factors ($k^* = 0.5$, $d^* = 10.0$).

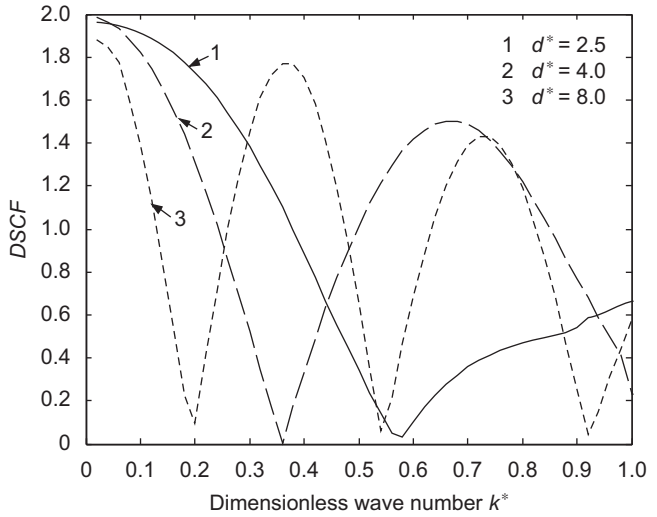

Fig. 3. Dynamic stress concentration factors versus dimensionless wavenumber with different values of d^* ($E_0 = \rho_0 = 0$, $\theta = \pi/2$).

with dots. The bold line obtained from the method in this paper represents the DSCFs in the thin plate without any inhomogeneities. Excellent agreement with Ref. [7] can be observed in Fig. 2. A thin plate without any inhomogeneities is identical to the plate with an inclusion which has the same mechanical properties and thickness as the plate itself. As expected, the DSCFs in this case are uniformly 1.0, and this also can validate the dynamical model.

Fig. 3 illustrates the DSCF at the position of $\theta = \pi/2$ as a function of the dimensionless wavenumber with $E_0 = h_0 = 0$. When the distance ratio is $d^* = 8.0$, the wave field close to the edge of the plate is almost the same as that of the semi-infinite plate with no inclusion. $E_0 = h_0 = 0$ means that the inclusion in the plate reduces to a cavity. From Fig. 3, one can see that when the incident wavenumber is $k^* \to 0$, the DSCF is the maximum, and its value is about $M_\theta^* = 1.90$, which is consistent with the numerical results of infinite plates in Refs. [18,22]. It can be seen that peaks and troughs occur in Fig. 3. This is due to the variation in wavenumber changing the distance between the inclusion and the nodal line in the total standing wave field created by the incident, reflected, and scattered waves. At some frequencies, the inclusion is at nodal line, while at others it is at an anti-nodal line.

Figs. 4–9 illustrate the angular distribution of DSCFs around the inclusion when the values of d^*, E^*, ρ^*, and v_0 are different.

In Fig. 4, the inclusion in the plate reduces to a cavity. From Fig. 4, it can be seen that when the distance between the inclusion and the semi-infinite edge is great, the dynamic stresses at the positions around the cavity show little variation. The dynamic stress at the positions of $\theta = 0$ is the maximum. If the distance between the inclusion and the semi-infinite edge becomes small, the DSCF at the position of $\theta = \pi$ is the maximum. The DSCF at the position of $\theta = 0$ is the minimum. The maximum value of DSCF is much greater than that at other positions.

In Fig. 5, the elastic modulus and density of the inclusion are greater than those of the plate. It can be observed that when the distance between the inclusion and the semi-infinite edge is small, the DSCF at the position of $\theta = \pi$ is still the maximum. Comparing the results with those in Fig. 4, it is clear that if the distance between the inclusion and the semi-infinite edge is great, the effects of the elastic modulus and density of the inclusion on the DSCFs are little. However, when the distance between the inclusion and the semi-infinite edge is small, the effects of the elastic modulus and density of the inclusion on the DSCFs become great, especially on the shadow side of the inclusion. Due to the effect of the elastic modulus and density of the inclusion, the dynamic stresses on the shadow side of the inclusion become great.

In Fig. 6, the elastic modulus and density of the inclusion are less than those of the plate. It can be observed that when the distance between the inclusion and the semi-infinite edge is small, the DSCF at the position of $\theta = \pi$ is still the maximum. Comparing the results with those in Fig. 4, it can be seen that if the distance

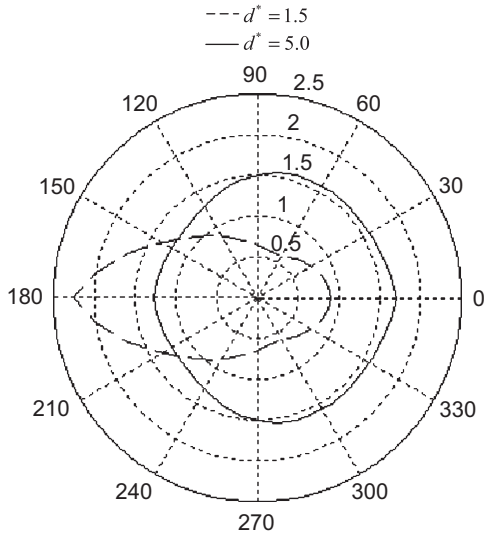

Fig. 4. Angular distribution of dynamic stress concentration factors around the cavity with different values of d^*; $k^* = 0.5$, $E_0 = \rho_0 = 0$.

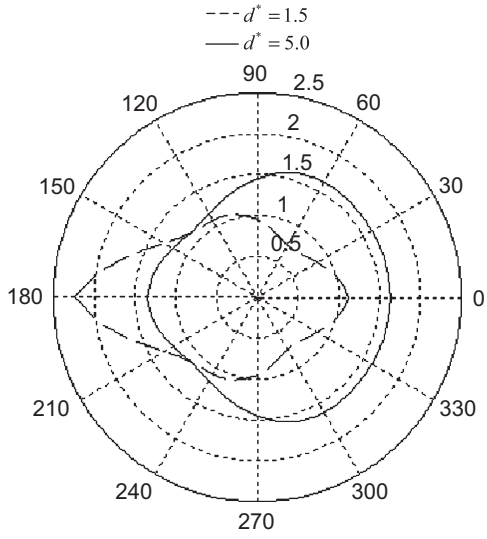

Fig. 5. Angular distribution of dynamic stress concentration factors around the inclusion with different values of d^*; $k^* = 0.5$, $E^* = 5.0$, $\rho^* = 2.0$, $h^* = 1.0$, $v = v_0 = 0.3$.

between the inclusion and the semi-infinite edge is great, the effects of the elastic modulus and density of the inclusion on the DSCFs are little. However, when the distance between the inclusion and the semi-infinite edge is small, the effects of the elastic modulus and density of the inclusion on the DSCFs become great, especially on the shadow side of the inclusion. Due to the effect of the elastic modulus and density of the inclusion, the dynamic stresses on the shadow side of the inclusion become little.

Comparing the results in Fig. 6 with those in Fig. 5, it is interesting to note that no matter whether the elastic modulus and density of the inclusion is greater than those of the plate, the dynamic stresses on the shadow side of the inclusion become great. When the distance between the inclusion and the semi-infinite edge is small, the dynamic stress on the position of $\theta = \pi$ is greater in the case of $E^* > 1.0$, $\rho^* > 1.0$ than that in the case of $E^* < 1.0$, $\rho^* < 1.0$. When the distance between the inclusion and the semi-infinite edge is great, the

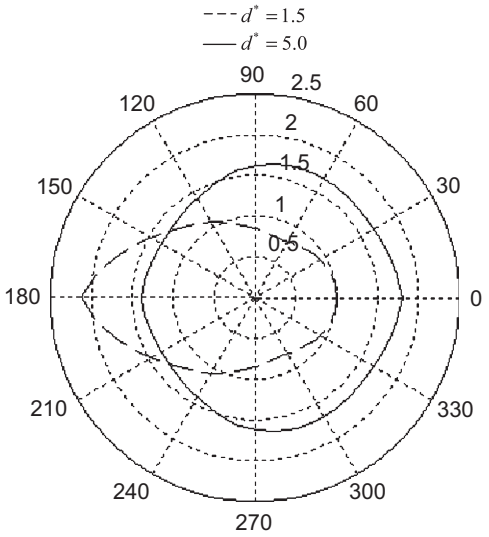

Fig. 6. Angular distribution of dynamic stress concentration factors around the inclusion with different values of d^*; $k^* = 0.5$, $E^* = 0.1$, $\rho^* = 0.2$, $h^* = 1.0$, $v = v_0 = 0.3$.

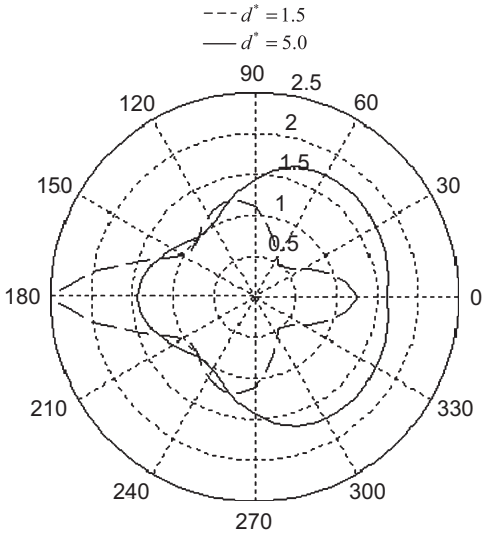

Fig. 7. Angular distribution of dynamic stress concentration factors around the inclusion with different values of d^*; $k^* = 0.5$, $E^* = 5.0$, $\rho^* = 2.0$, $h^* = 1.5$, $v = v_0 = 0.3$.

dynamic stress on the position of $\theta = 0$ becomes greater in the case of $E^* < 1.0$, $\rho^* < 1.0$ than that in the case of $E^* > 1.0$, $\rho^* > 1.0$.

The effect of increasing the thickness of the inclusion on the angular distribution of DSCF is shown in Fig. 7. It can be seen that when the distance between the inclusion and the semi-infinite edge is small, due to the effect of the thickness of the inclusion, the dynamic stress on the shadow side of the inclusion become much greater, especially at the position of $\theta = \pi$. However, if the distance between the inclusion and the semi-infinite edge is great, the dynamic stresses on the illuminated side of the inclusion become much greater. The dynamic stresses at the positions of $\theta = \pi/2$ and $-\pi/2$ show little variation with the thickness of the inclusion.

The effect of Poisson's ratio of the inclusion on the angular distribution of DSCF is shown in Figs. 8 and 9. In Fig. 8, Poisson's ratio of the inclusion is greater than that of the plate. In Fig. 9, Poisson's ratio of the

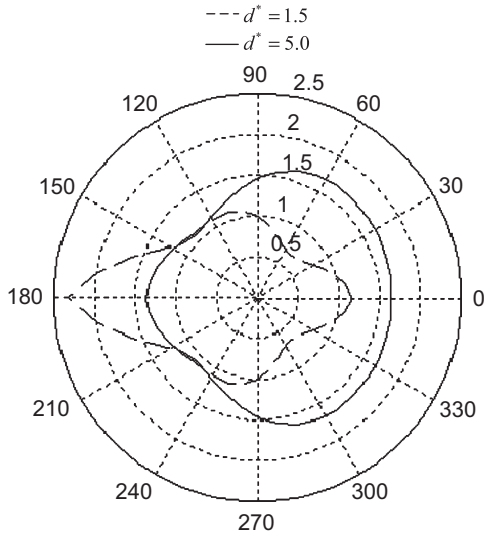

Fig. 8. Angular distribution of dynamic stress concentration factors around the inclusion with different values of d^*; $k^* = 0.5$, $E^* = 5.0$, $\rho^* = 2.0$, $h^* = 1.0$, $v = 0.3$, $v_0 = 0.2$.

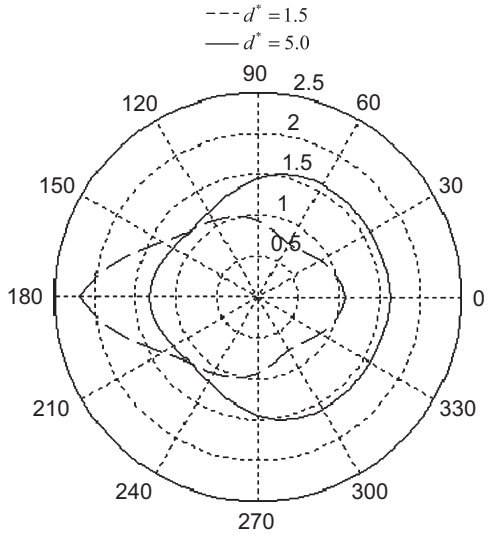

Fig. 9. Angular distribution of dynamic stress concentration factors around the inclusion with different values of d^*; $k^* = 0.5$, $E^* = 5.0$, $\rho^* = 2.0$, $h^* = 1.0$, $v = 0.3$, $v_0 = 0.4$.

inclusion is less than that of the plate. Comparing the results with those in Fig. 5, it can be seen that only if the distance between the inclusion and the semi-infinite edge is small, does a change of the inclusion's Poisson's ratio have any observable effect of on the DSCFs around the inclusion. The effect at the position of $\theta = \pi$ is the maximum. When Poisson's ratio of the inclusion is greater than that of the plate, the dynamic stress becomes small. When Poisson's ratio of the inclusion is less than that of the plate, the dynamic stress becomes great.

Fig. 10 illustrates the DSCFs at the position of $\theta = \pi/2$ of the inclusion as a function of the incident wavenumber when the values of E^* and ρ^* are different. It can be seen that the dynamic stress at the position of $\theta = \pi/2$ decreases with the increase of dimensionless wavenumber. In the region of low frequency, the

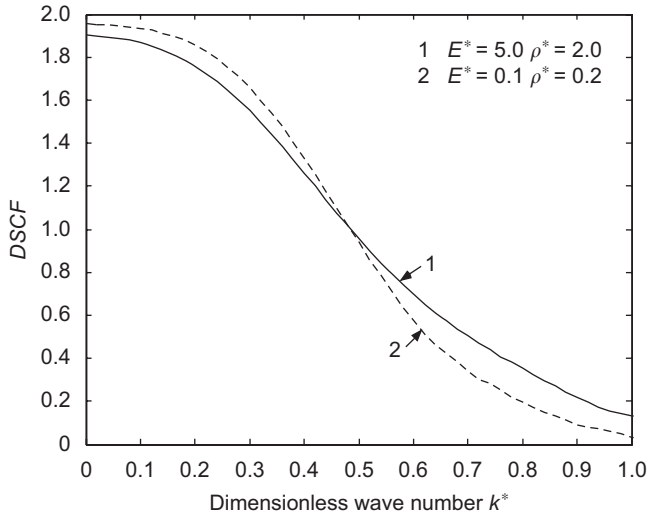

Fig. 10. Dynamic stress concentration factors versus dimensionless wavenumber with different values of E^* and ρ^* at $\theta = \pi/2$ ($h^* = 1.0$, $d^* = 1.5$, $v = v_0 = 0.3$).

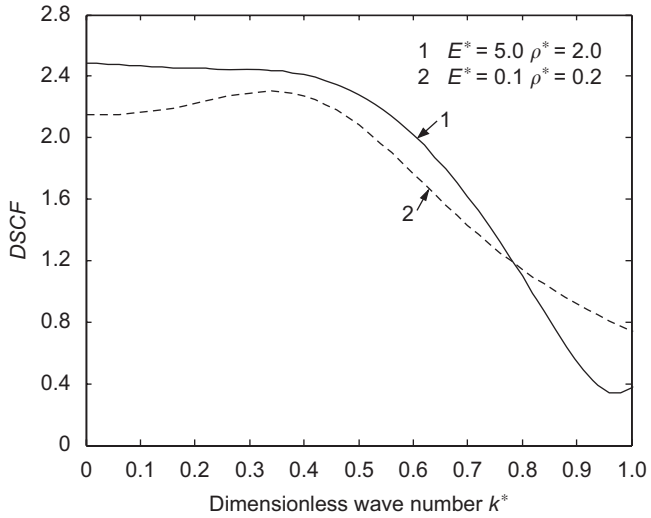

Fig. 11. Dynamic stress concentration factors versus dimensionless wavenumber with different values of E^* and ρ^* at $\theta = \pi$ ($h^* = 1.0$, $d = 1.5$, $v = v_0 = 0.3$).

dynamic stress decreases with the increase of the values of E^* and ρ^*. In the region of higher frequency, the dynamic stress increases with the increase of the values of E^* and ρ^*.

Fig. 11 illustrates the DSCFs at the position of $\theta = \pi$ of the inclusion as a function of the incident wavenumber when the values of E^* and ρ^* are different. It can be seen that the dynamic stress at the position of $\theta = \pi$ decreases with the increase of dimensionless wavenumber. In the region of low frequency, the dynamic stress increases with the increase of the values of E^* and ρ^*. In the region of higher frequency, the dynamic stress decreases with the increase of the values of E^* and ρ^*. Comparing with the results in Fig. 10, it is observed that the effect of the values of E^* and ρ^* on the dynamic stress at the position of $\theta = \pi$ is greater.

Figs. 12 and 13 illustrate the DSCFs as a function of the incident wavenumber with different values of v_0 at the positions of $\theta = \pi/2$ and π of the inclusion, respectively. It can be seen that in the region of low frequency,

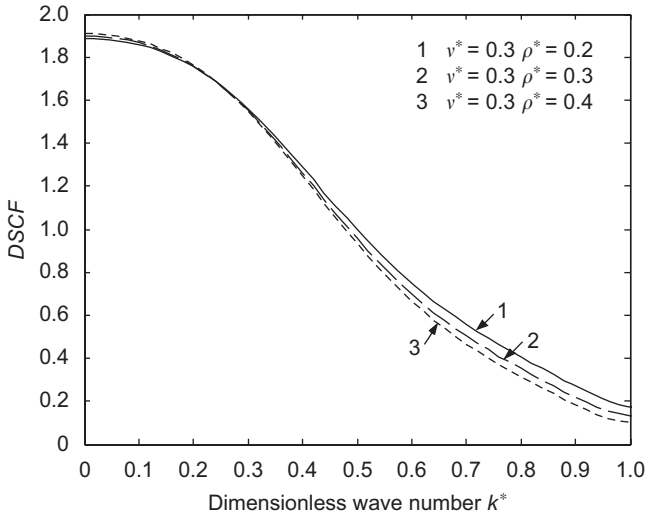

Fig. 12. Dynamic stress concentration factors versus dimensionless wavenumber with different values of v_0 at $\theta = \pi/2$ ($E^* = 5.0$, $\rho^* = 2.0$, $h^* = 1.0$, $d^* = 1.5$).

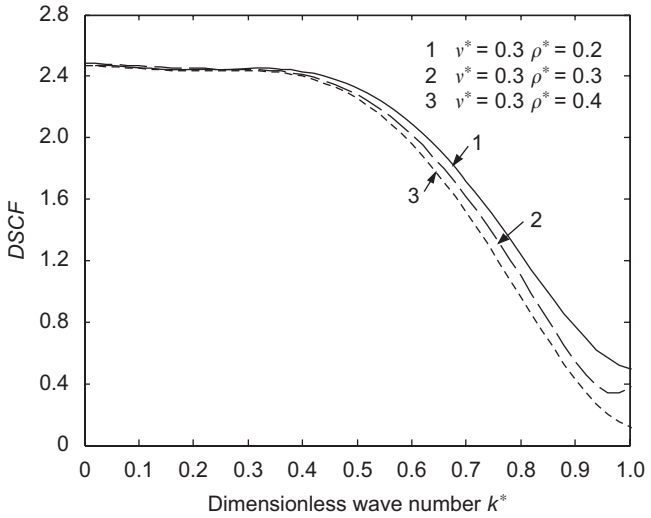

Fig. 13. Dynamic stress concentration factors versus dimensionless wavenumber with different values of v_0 at $\theta = \pi$ ($E^* = 5.0$, $\rho^* = 2.0$, $h^* = 1.0$, $d^* = 1.5$.

the dynamic stress shows little variation with the value of v_0. However, in the region of higher frequency, the dynamic stress decreases with the increase of the value of v_0. Comparing the results in Figs. 12 and 13, it is observed that the effect of the value of v_0 on the dynamic stress at the position of $\theta = \pi$ is greater.

Figs. 14 and 15 illustrate the DSCFs as a function of the incident wavenumber with different values of h^* at the positions of $\theta = \pi/2$ and π of the inclusion, respectively. At the position of $\theta = \pi/2$, the dynamic stress increases with the increase of the value of h^* in the region of higher frequency; the dynamic stress shows little variation in the region of low frequency. However, at the position of $\theta = \pi$, the dynamic stress increases greatly with the increase of the value of h^* in the region of low frequency; the dynamic stress shows little variation in the region of higher frequency. Comparing the results in Figs. 14 and 15, it is observed that the effect of the value of h^* on the dynamic stress at the position of $\theta = \pi$ is greater.

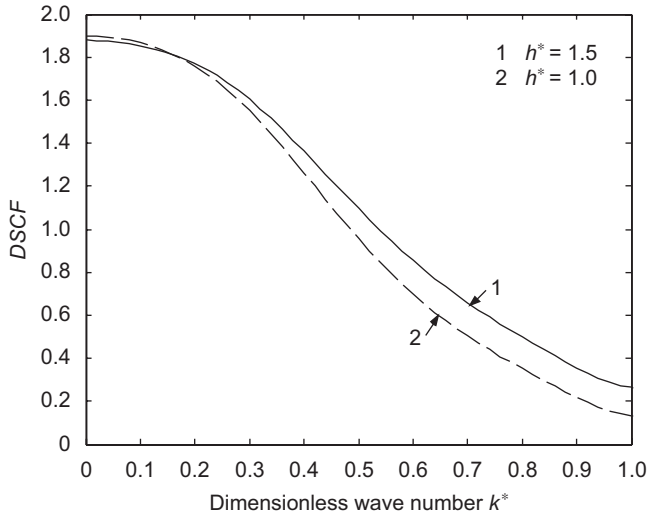

Fig. 14. Dynamic stress concentration factors versus dimensionless wavenumber with different values of h^* at $\theta = \pi/2$ ($E^* = 5.0$, $\rho^* = 2.0$, $v = v_0 = 0.3$, $d^* = 1.5$).

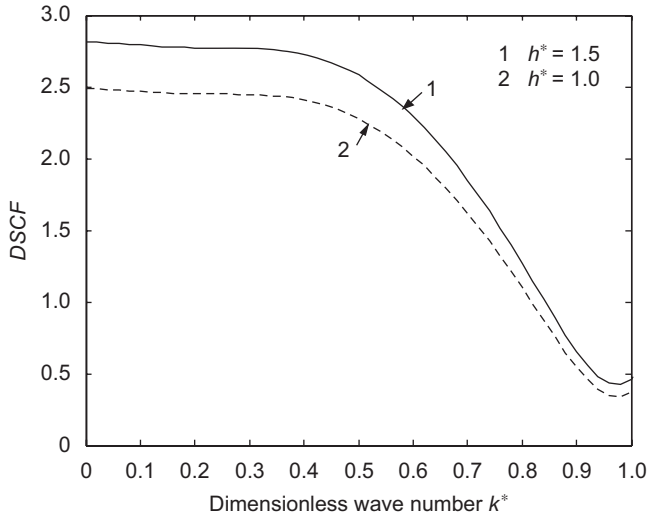

Fig. 15. Dynamic stress concentration factors versus dimensionless wavenumber with different values of h^* at $\theta = \pi$ ($E^* = 5.0$, $\rho^* = 2.0$, $v = v_0 = 0.3$, $d^* = 1.5$).

7. Conclusion

In this study, based on the dynamical equation of flexural waves in elastic thin plates, and applying the image method and the wave function expansion method, the multiple scattering of flexural waves and dynamic stress from a cylindrical inclusion in a semi-infinite thin plate are investigated. The semi-infinite edge with roller-supported boundary conditions is considered. Analytical solutions and numerical results of the problem are presented and analyzed. Comparisons with previous literature demonstrate the validity of the analytical method.

It can be seen that the analytical results of dynamic stress in semi-infinite plates are different from those in infinite plates. Comparing with the results in Hu et al. [18], the existence of the inclusion has great effect on the distribution of the dynamic stress in the semi-infinite plate, especially in the region of higher frequency. If the distance between the inclusion and the semi-infinite edge is small, due to the multiple scattering of elastic

waves, the DSCF at the position of $\theta = \pi$ around the inclusion is the maximum. The effects of the elastic modulus, density, thickness, and Poisson's ratio of the inclusion on the DSCFs are greater when the distance between the inclusion and the semi-infinite edge is small, especially on the shadow sides of the inclusion. In contrast to the elastic modulus, density, thickness of the inclusion, the effect of Poisson's ratio of the inclusion on the angular distribution of DSCF is less.

The analysis of this paper can provide a theoretical basis and reference data for strength designs and non-destructive evaluation of plate structures with holes near their edges.

References

[1] G. Kirsch, Die Theorie der Elastizität und die Bedürfnisse der Festigkeitslehre, *Zeitshrift des Vereines deutscher Ingenieure* 42 (1898) 797–807.
[2] C.F. Ying, R. Truell, Scattering of a plane longitudinal wave by a spherical obstacle in an isotropically elastic solid, *Journal of Applied Physics* 27 (1956) 1086–1097.
[3] K. Kato, Reflection of sound wave due to a hollow cylinder in an elastic body, *Memoirs of the Institute of Scientific and Industrial Research, Osaka University, Japan* 9 (1952) 16–27.
[4] R.M. White, Elastic wave scattering at a cylindrical discontinuity in a solid, *Journal of the Acoustical Society of America* 30 (1958) 771–785.
[5] Y.H. Pao, C.C. Chao, Diffractions of flexural waves by a cavity in an elastic plate, *AIAA Journal* 2 (1964) 2004–2010.
[6] Y.H. Pao, Dynamic stress concentration in an elastic plate, *Journal of Applied Mechanics—Transactions of the ASME* 29 (1962) 299–305.
[7] R. Paskaramoorthy, A.H. Shah, S.K. Datta, Scattering of flexural waves by cavities in a plate, *International Journal of Solids and Structures* 25 (1989) 1177–1191.
[8] R. Paskaramoorthy, A.H. Shah, S.K. Datta, Scattering of flexural waves by a crack in a plate, *Engineering Fracture Mechanics* 33 (1989) 589–598.
[9] C. Vemula, A.N. Norris, Flexural wave propagation and scattering on thin plates using Mindlin theory, *Wave Motion* 26 (1997) 1–12.
[10] C. Vemula, A.N. Norris, Scattering of flexural waves on thin plates, *Journal of Sound and Vibration* 181 (1) (1995) 115–125.
[11] Y. Leviatan, E.T. Erez, M.J. Beran, A source-model technique for analysis of flexural wave scattering in a heterogeneous thin plate, *Quarterly Journal of Mechanics and Applied Mathematics* 45 (1992) 499–514.
[12] E.M. Salame, Stress distribution around a circular inclusion in a semi-infinite elastic plate, *Journal of Applied Mechanics—Transactions of the ASME* 25 (1958) 125–135.
[13] A.H. Shah, K.C. Wong, S.K. Datta, Surface displacements due to elastic wave scattering by buried planar and non-planar cracks, *Wave Motion* 7 (1985) 319–333.
[14] X.-Q. Fang, C. Hu, S.Y. Du, Strain energy density of a circular cavity buried in a semi-infinite functionally graded material subjected to shear waves, *Theoretical and Applied Fracture Mechanics* 46 (2006) 166–174.
[15] X.-Q. Fang, C. Hu, W.-H. Huang, Dynamic stress of a circular cavity buried in a semi-infinite functionally graded piezoelectric material subjected to shear waves, *European Journal of Mechanics A/Solids* 26 (2007) 1016–1028.
[16] X.-Q. Fang, C. Hu, W.-H. Huang, Strain energy density of a circular cavity buried in a semi-infinite slab of functionally graded materials subjected to anti-plane shear waves, *International Journal of Solids and Structures* 44 (2007) 6987–6998.
[17] K.F. Graff, *Wave Motions in Elastic Solids*, Dover, New York, 1991.
[18] C. Hu, X.-Q. Fang, W.-H. Huang, Multiple scattering of flexural waves in a semi-infinite thin plate with a cutout, *International Journal of Solids and Structures* 44 (2007) 436–446.
[19] X.-Q. Fang, C. Hu, D.-B. Wang, Multiple scattering of flexural waves from two cutouts in a semi-infinite thin plate, *International Journal of Solids and Structures* 45 (2008) 4236–4246.
[20] Lord Rayleigh, *The Theory of Sound*, Vol. 1, Macmillan, New York, 1877 reprinted 1945 by Dover Publications.
[21] M.A. Abramowitz, I.A. Stegun, *Handbook of Mathematical Functions*, Natl. Bur. Stand, Washington, DC, 1964.
[22] Y.H. Pao, C.C. Mow, *Diffraction of Elastic Waves and Dynamic Stress Concentrations*, Crane, Russak, New York, 1973.